Journal of Materials Chemistry B

Accepted Manuscript

ROYAL SOCIETY OF CHEMISTRY

www.rsc.org/materialsB

Journal Name

ARTICLE

A two-photon fluorescent RNA probe screened from a series of oxime-functionalized 2,2':6',2''-terpyridine ZnX_2 (X = Cl, Br, I) complexes

Received 00th January 20xx,
Accepted 00th January 20xx

DOI: 10.1039/x0xx00000x

www.rsc.org/

Hui Wang[a], Xiaohe Tian*[b], Wei Du[a], Qiong Zhang[a], Lijuan Guan[c], Aidong Wang[d], Yujin Zhang[e], Chuankui Wang[e], Hongping Zhou[a], Jieying Wu*[a], Yupeng Tian[a,f]

Imaging RNA in living cells is a powerful tool to understand intracellular RNA function. Therefore, an effective two-photon fluorescent probe with reasonable two-photon action cross-section to label RNA is now urgently required. In this work, a series of novel two-photon absorbing terpyridine ZnX_2 (X=Cl, Br, I) complexes have been designed and an effective RNA imaging probe has been obtained. The results revealed that **OTP-$ZnCl_2$** possesses a large Stokes shift and two-photon action cross section. Furthermore, live cell imaging experiments indicated that **OTP-$ZnCl_2$** could stain nucleoli in living cells by binding with nucleoli RNA. The mechanism of selective nucleoli staining of **OTP-$ZnCl_2$** was studied systemically *via* both experiments and molecular modeling calculations. Due to its low cytotoxicity, good membrane permeability and counterstain compatibility with the commercial fluorescent nucleic dye Hoechst 33342, as well as the ability to label RNA in living cells, **OTP-$ZnCl_2$** is a promising candidate for the detection of nucleic acid in living cells.

1. Introduction

Nucleic acids (NAs), such as DNA (deoxyribonucleic) and RNA (ribonucleic acid), are biological macromolecules that function in encoding, transmitting and expressing genetic information, and play an important role in biological system.[1-5] Therefore, fluorescent imaging of RNA *in vitro* and *in vivo* is of great significance in biochemistry and biomedicine.[6,7] However, the use of currently available RNA probe "Syto RNA-select" has suffered from high cytotoxicity and photo-bleaching as well as the small Stokes shifts, which lead to an unwanted background noise ascribed to the auto-fluorescence from endogenous fluorophores.[8-12] Two-photon microscopy (2PM) has been reported to be able to penetrate into deeper tissues and generate an autofluorescence-free background,[13-17] making it a promising approach to selectively detect RNAs in living samples. Therefore, RNA-specific two-photon fluorescent probes with optimize biocompatibility and two-photon action cross-section are believed to be the next ideal RNA imaging systems.

Luminescent metal complexes have emerged as an important class of imaging agents, because of their photophysical properties such as high luminescence, good photostability, long lifetime, large Stokes shift and large two-photon absorption cross section.[18] Moreover, luminescent metal complexes have greater flexibility and structural diversity, comparing to organic fluorophores.[19] Therefore, numerous studies have been focused on luminescent d^6 metal complexes such as Ir,[20,21,22] Ru,[23,24,25,26] and d^8 metal complexes Pt,[27,28] which had been made to demonstrate their advantages. To avoid the potential toxicity from heavy metals, and the possible involvement of active oxygen species during light irradiation, we turned our attention to d^{10} metal Zn (II) complex, which is a biocompatible

[a] Department of Chemistry, Key Laboratory of Functional Inorganic Material Chemistry Anhui Province, Anhui University, Hefei 236001, P.R. China
[b] School of Life Science, Anhui University, Hefei 230601, P.R. China
[c] Department of Chemistry, University College London, WC1H0AJ, UK
[d] Huangshan College, Huangshan, China
[e] College of Physics and Electronics, Shandong University, Jinan 250014, China
[f] State Key Laboratory of Coordination Chemistry, Nanjing University, Nanjing 210093, P.R. China
† Corresponding author. Tel: +86-551-63861227
Email address: t.xiaohe@ucl.ac.uk; jywu1957@163.com

metal that widely exists in metalloenzymes and has a closed-shell electronic configuration to produce fluorescence characteristics depending on the ligand. Moreover, as the second most abundant transition metal ion and essential trace element in the human body, Zn (II) possesses low cytotoxicity and smaller molecular weight than heavy metal complexes (e.g. Ir^{III}, Ru^{II} and Pt^{II}). In 2007, Pascu's group reported a Zn (II) bis(thisosemicarbazonato) complex, which is the first example of a Zn (II) complex in cell imaging.[29] Recently, Zhang and co-worker's described a ranges of ZnSalen/Salophen complexes, which possess high luminescence, large two-photon cross section and low cytotoxicity.[18,30] In our previous work, we have reported a cell-permeable terpyridine Zn(II) complexes.[31,32] However, according to our knowledge, the interaction between Zn (II) complexes with RNA in living cells has been rarely reported.

Herein, according to the idea mentioned above, a series of novel terpyridine ZnX_2 (X=Cl, Br, I) complexes were designed and synthesized **(Scheme 1)**. This design is based on the following considerations: (1) oxime is the most stable imines leading to its wide use in protein labelling, analysis of protein-protein interactions and in in-vivo cell imaging. We assumed that the oxime group might be able to form hydrogen bonds with nucleic acids in cells. (2) triphenylamine moiety with a strong electron donor and efficient π-electron bridge, as a building block has been used to develop 2PA chromophores. (3) terpyridine and its derivatives represent an important class of ligands in the fields of coordination chemistry, which have excellent optical properties and extremely strong binding affinity towards most transition metal ions.[33-35] (4) halide elements can influence the photophysical and photochemical properties of the complexes to be coordinated with, as well as their molecular polarity and size. The photophysical property of the complexes was investigated systematically comparing to their free ligands. Relying on the comprehensive studies, it was found that **OTP-$ZnCl_2$** could penetrate through the nuclear membrane and strongly interact with RNA both within nucleoli and cytoplasm, all suggesting that it is a potential two-photon fluorescent RNA probe for in vitro and in vivo bioimaging.

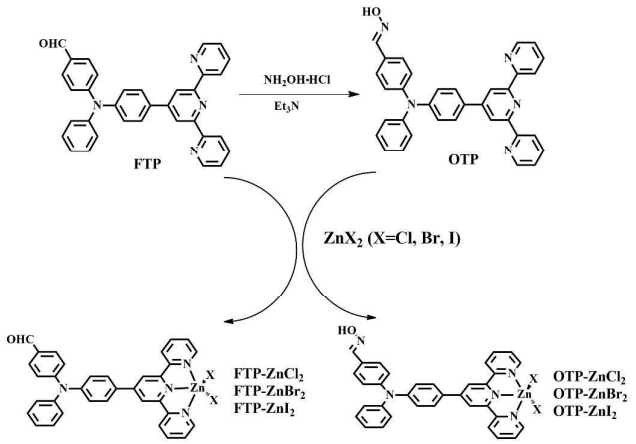

Scheme 1 The synthetic routes of the ligands **FTP**, **OTP** and their ZnX_2 (X=Cl, Br, I) complexes.

2. Results and discussion

2.1 Crystal structure

The unit cell, data collection, and refinement parameters were located in **Table S1**. Selected bond distances and angles were listed in **Table S2-S7**.

Structures of OTP

Ligand **OTP** crystallizes in the triclinic crystal system with the Pī space group. The dihedral angles between the central pyridyl and two neighboring pyridyl ring planes are 11.32° and 12.99°, respectively, indicating that the terpyridyl group is barely coplanar. The dihedral angle between the benzene ring and the core pyridine of the terpyridine group is 31.25°, which is linked by C8-C16 (1.475 Å) with conjugated bond length. The planarity and the conjugated geometric configuration indicates that the ligand **OTP** has delocalized π-electron system.

Structures of Zn(II) complexes

As shown in **Fig 1**, the metal Zn (II) center adopts a distorted trigonal bipyramidal N_3X_2 (X=Cl, Br, I) coordination. The bond lengths of Zn-X (X=Cl, Br, I) in these complexes are in the 2.256-2.574 Å range, showing that there is a higher degree of electron delocalization in the Zn-tpy complexes. The Zn-N bond lengths in these complexes are within the range of

2.091-2.234 Å, whereas in related references they are in the range of 1.992-2.234 Å.[31] The dihedral angles between the central pyridyl and its two neighboring pyridyl ring planes are nearly coplanar. Those structural features show that there is a higher degree of electron delocalization favoring NLO response.

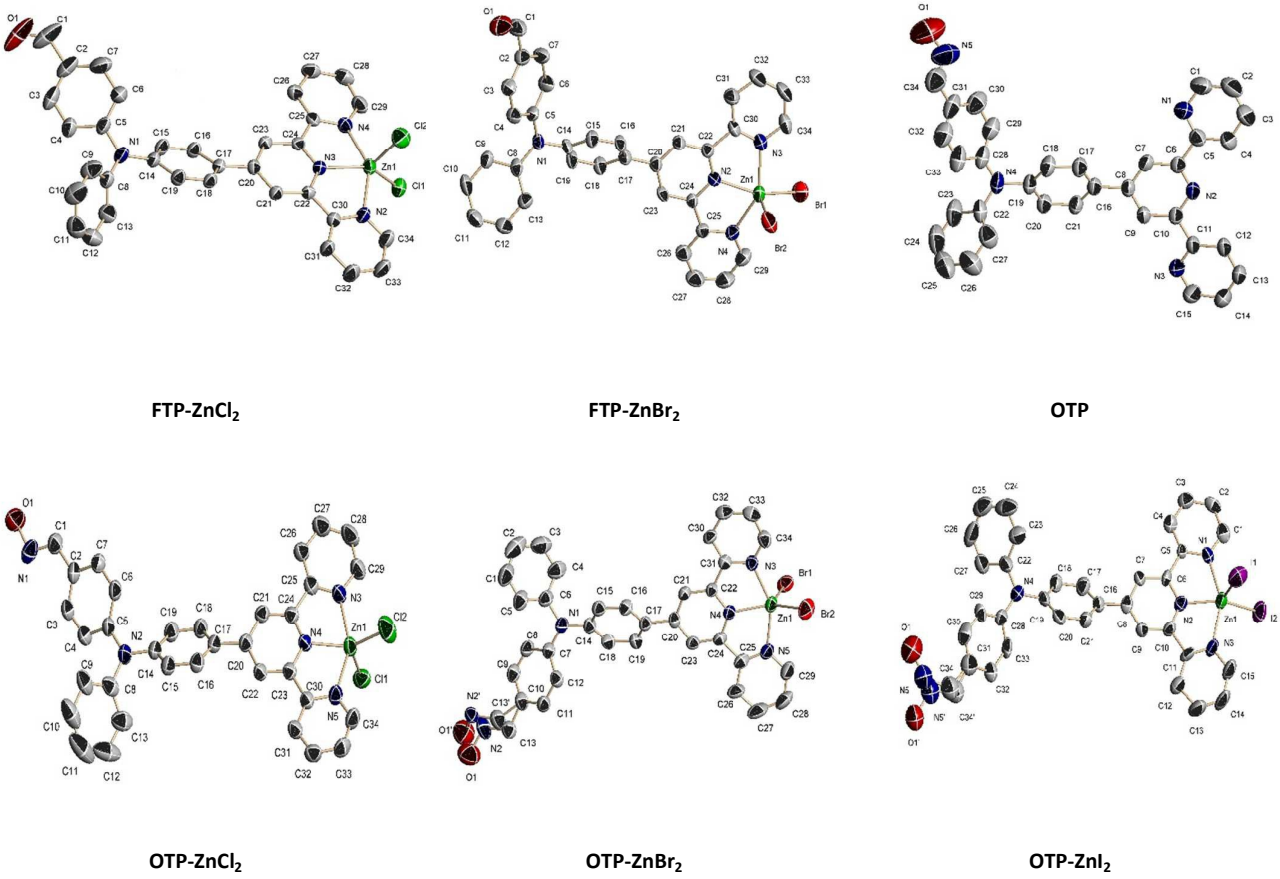

FTP-ZnCl$_2$ **FTP-ZnBr$_2$** **OTP**

OTP-ZnCl$_2$ **OTP-ZnBr$_2$** **OTP-ZnI$_2$**

Fig. 1 The crystal structures of **FTP-ZnX$_2$** (X=Cl, Br), **OTP** and **OTP-ZnX$_2$** (X=Cl, Br, I). All H atoms and solvent molecules have been omitted for clarity.

2.2 Optical properties

The photophysical properties of all the compounds were summarized in **Table S8** (corresponding figures were given in supporting information).

Linear absorption properties

The UV-vis absorption spectra of the compounds were shown in **Fig 2**, from which it can be seen that the ligands **FTP** and **OTP** both exhibited two absorption bands in CH_3CN solution. The higher energy band was assigned to the $\pi_{terpyridine}$ -$\pi^*_{terpyridine}$ transitions,[36] while the lower energy band was assigned to the intramolecular charge transfer (ICT) transition. Three main bands were observed for all the Zn (II) complexes. The highest energy band (280 nm) was assigned to the $\pi_{terpyridine}$ -$\pi^*_{terpyridine}$ transitions, which is in accord with the ligands. The mediate band at 330 nm was assigned to the ICT transition, while the lowest energy band at about 400 nm was assigned to ligand-to-ligand charge transfer (LLCT) transition between the sub-ligand X (X = Cl, Br, I) and the ligand, which was further confirmed by time-dependent density functional theory (TD-DFT) calculations (**Fig S3-S6** and **Table S9**).

As shown in **Fig S1**, for **OTP**, weak solvatochromism was observed in the absorption bands, indicating that the little difference in dipoles between the ground and excited state of the chromophores. Moreover, the maximum UV-vis absorption bands (λ_{max}) of the complexes shown in **Fig 2** displayed a red-shift in the order of **FTP-ZnCl$_2$ < FTP-ZnBr$_2$ < FTP-ZnI$_2$**. Similar order

was also observed for complexes **OTP-ZnCl$_2$, OTP-ZnBr$_2$** and **OTP-ZnI$_2$**, which should result from the increased polarizability of Cl, Br and I, lowering the energy of the whole molecule at the corresponding level.

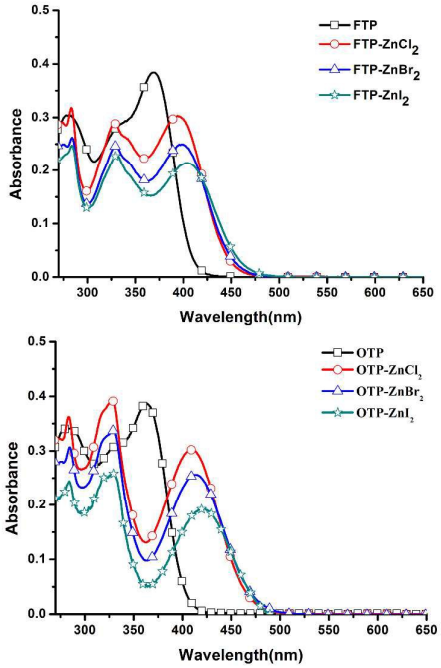

Fig. 2 Linear absorption spectra of the ligands **FTP**, **OTP** and their ZnX_2 (X=Cl, Br, I) complexes in CH_3CN solvent (c=10 μM).

One-photon excited fluorescence (OPEF) properties

By the comparison of ligands **FTP** and **OTP**, the fluorescent peaks of their corresponding ZnX_2 (X=Cl, Br, I) complexes undergo an obvious red-shift as shown in **Table S9**, which may be assigned to LLCT. For the series of **OTP-ZnX$_2$** (X=Cl, Br, I), in high polar solvent DMF, the maximal emission wavelength was blue-shifted comparing to those non-polar solvent benzene. Such behavior is consistent with a symmetry breaking in the ground state. When molecule with D-A structural model is in a high polar solvent, the molecule tends to polarized from the ground state to form a charge-separated molecule by the action of an electric field caused by the surrounding solvent molecules. With the increasing polarity of the solvents, the fluorescence lifetime of **OTP, FTP-ZnCl$_2$, FTP-ZnBr$_2$** and **FTP-ZnI$_2$** increased except in ethanol and acetonitrile, while the fluorescence lifetime of **OTP-ZnCl$_2$, OTP-ZnBr$_2$** and **OTP-ZnI$_2$** decreased except in DMF. The fluorescence lifetimes of **OTP-ZnX$_2$** (X=Cl, Br, I) were a little longer than that of its free ligand **OTP** (4.46 ns), which is consistent with inter-system crossing being very rapid due to the strong spin-orbital coupling induced by the mixing of the ligand (π and π*) and metal dπ orbitals.[31] Then, the emission lifetime τ was further calculated using the Einstein transition properties according to the formula (in a.u.) as follows.

$$\tau = \frac{c^3}{2(E_{flu})^2 \delta_{op}}$$

Where c is the velocity of light, E_{flu} is the transition energy, and δ_{op} is the oscillator strength. The calculated fluorescence lifetimes of **FTP**, **OTP, FTP-ZnX$_2$** and **OTP-ZnX$_2$** (X=Cl, Br, I) were 2.18, 3.17, 4.21, 4.13, 4.08, 3.36, 3.18 and 3.34 ns, respectively, being consistent with the experimental ones.

In order to further demonstrate the influence of the solvents on fluorescence, the Stokes' shifts of **FTP**, **OTP, FTP-ZnX$_2$** and **OTP-ZnX$_2$** (X=Cl, Br, I) in solvents of different polarity were listed in **Table S8**. The Stokes' shifts are defined as the loss of energy between the absorption and reemission of light, which contain several dynamic processes, including the energy loss due to the dissipation of vibrational energy, the redistribution of electrons in surrounding solvent molecules induced by the altered dipole moment of the excited chromophore, the reorientation of the solvent molecules around the excited state dipole, and specific interactions between the fluorophore and solvent or solutes. The Lippert-Mataga equation is the most widely accepted equation to evaluate the dipole moment changes of the dyes with photoexcitation.[37,38] Plots of the Stokes shifts as a function of the solvent polarity factor Δ*f* were shown in **Fig. S7**. Only the data involving the aprotic solvents were shown here because the application of this analysis with solvents where specific solute-solvent interactions are present is not appropriate. As shown in **Fig. S7**, the Lippert-Mataga plot of complex **FTP-ZnCl$_2$** gave much higher slope than its free ligand and the other complexes, which implies more dipole moment changes for **FTP-ZnCl$_2$** with photoexcitation.[38] In addition, the Lippert-Mataga plot of **OTP** also presented much higher slope

than its Zn (II) complexes. The slope of the best-fit line was related to the dipole moment change between the ground and excited states (μ_e-μ_g). The slopes of all eight lines were 8236, 10793, 9624, 8633, 9290, 5492, 3769 and 5198 cm^{-1} for **FTP**, **OTP, FTP-ZnX$_2$** and **OTP-ZnX$_2$** (X=Cl, Br, I), respectively. As a result, the values of μ_e-μ_g were calculated as 13.2 D for **FTP**, 16.1 D for **OTP**, 16.4 D for **FTP-ZnCl$_2$**, 14.6 D for **FTP-ZnBr$_2$**, 15.1 D for **FPT-ZnI$_2$**, 11.6 D for **OPT-ZnCl$_2$,** 9.1 D for **OTP-ZnBr$_2$,** and 12.1 D for **OTP-ZnI$_2$,** respectively. The highest value with **FTP-ZnCl$_2$** indicated that the molecule in the excited state has an extremely polar structure, corresponding to its linear and nonlinear optical properties.[31]

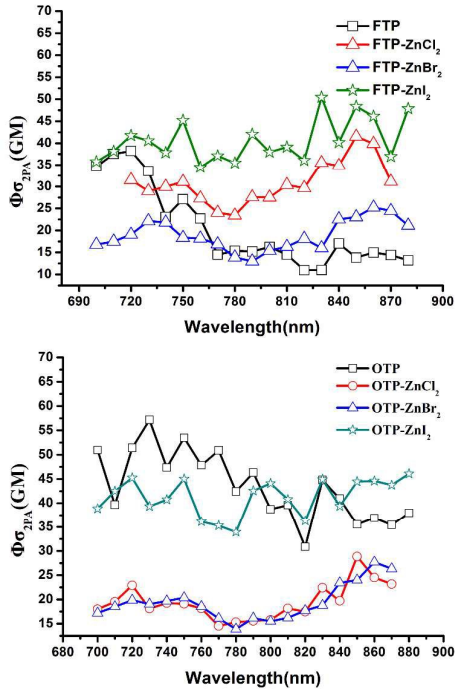

Fig. 3 Two-photon action absorption cross-sections of **FTP**, **OTP** and their ZnX_2 (X=Cl, Br, I) complexes in DMF solution.

2.3 Two-photon absorption cross sections

Before further exploring their bio-imaging application, the two-photon action absorption cross-sections of all compounds were detected in the wavelength range 700 to 870 nm in DMF solution by the two-photon-induced fluorescence assay using fluorescein as the standard (**Fig 3**). To eliminate the contributions from the excited-state absorption, a femtosecond (~ 140 fs) pulsed laser was used in the measurements. Detailed procedures have been described in our previous work.[39,40] The maximum two-photon action absorption cross-sections ($\Phi\sigma_{2PA}$) are 38.2 GM for **FTP**, 57.2 GM for **OTP**, 41.5 GM for **FTP-ZnCl$_2$**, 25.2 GM for **FTP-ZnBr$_2$,** 50.5 GM for **FTP-ZnI$_2$**, 28.8 GM for **OTP-ZnCl$_2$**, 27.7 GM for **OTP-ZnBr$_2$,** and 46.1 GM for **OTP-ZnI$_2$**. This means all the compounds possess 2PA response, highlighting their potential applications in 2PA imaging.

2.4 Selectively of Zn (II) complexes towards nucleic acids in solution

The interaction of all compounds with NA were preliminary studied by one-photon fluorescence spectra. As shown in **Fig 4**, all compounds showed a stronger interaction with NA except **FTP** and **OTP**. Significantly, **OTP-ZnCl$_2$** has a higher response to RNA than to DNA. In the following experiments, we focus on **OTP-ZnCl$_2$**.

The fluorescence properties of **OTP-ZnCl$_2$** interacting with RNA and DNA were investigated (**Fig 5**). Upon the addition of NA at a 200:1 ratio, the fluorescence intensity of **OTP-ZnCl$_2$** showed an approximately 2.74-fold and 1.23-fold enhancement with the presence of RNA and DNA, respectively (**Fig 5a**). In the two-photon fluorescence spectra, the fluorescence in the presence of RNA was stronger than that in the presence of DNA (**Fig 5b**). A similar trend was observed in the one- and two-photon fluorescence of **OTP-ZnCl$_2$** with the addition of NA, which highly indicate that **OTP-ZnCl$_2$** has better interacts with RNA than DNA.

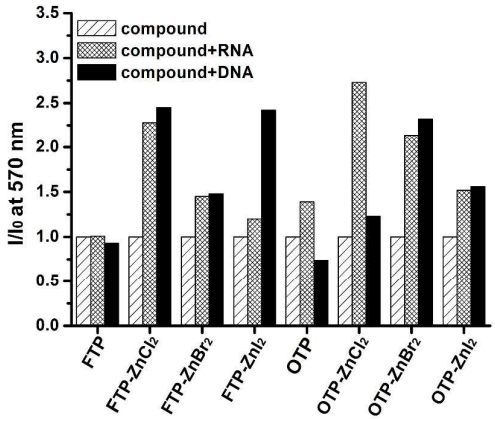

Fig. 4 Relatively fluorescence intensity of **FTP**, **OTP** and their ZnX_2 (X=Cl, Br, I) complexes upon addition of DNA and RNA. Compounds concentration: 10 μM. NA concentration: 2 mM.

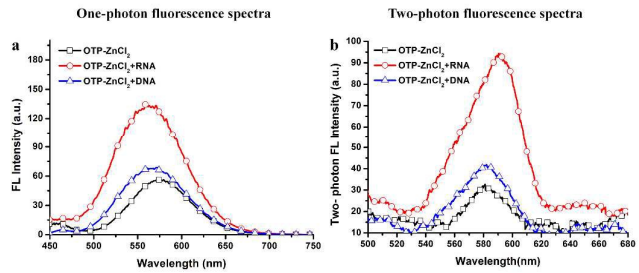

Fig. 5 The fluorescence enhancements of **OTP-ZnCl$_2$** upon addition of RNA and DNA. (a) The one-photon fluorescence spectra of **OTP-ZnCl$_2$** (10 μM), **OTP-ZnCl$_2$** (10 μM) + **RNA** (2 mM) and **OTP-ZnCl$_2$** (10 μM) + **DNA** (2 mM). (b) The two-photon fluorescence spectra of **OTP-ZnCl$_2$** (0.1 mM), **OTP-ZnCl$_2$** (0.1 mM) + **RNA** (20 mM) and **OTP-ZnCl$_2$** (0.1 mM) + **DNA** (20 mM).

The mechanism of the light-switch effect of **OTP-ZnCl$_2$** when binding to RNA could be explained by two factors. Firstly, **OTP-ZnCl$_2$** molecule was non-emissive when it was in a twist intramolecular charge transfer (TICT) state where non-radiative process quenches the fluorescence; inversely, when the formation of TICT state was restricted, the complex became brightly luminescent unit. Once in water, the larger dipole moment in the excited state interacts strongly with the polar solvent, leading to the charge separation and consequently the formation of TICT state. However, the formation of TICT state was restricted when **OTP-ZnCl$_2$** was protected from water in the grooves of RNA. Eventually, the fluorescence of **OTP-ZnCl$_2$** would be restored. Secondly, the weak emission of **OTP-ZnCl$_2$** in water could be attributed to the rapid non-radiative decay that results from the collisional interactions and the torsional motion of fluorophore responsive to the low quantum yield. When binding to RNA, the torsional motion of C-C single bond and triphenylamine group can be restricted by the steric effect derived from the hydrogen interactions, thus enhancing the fluorescence intensity.

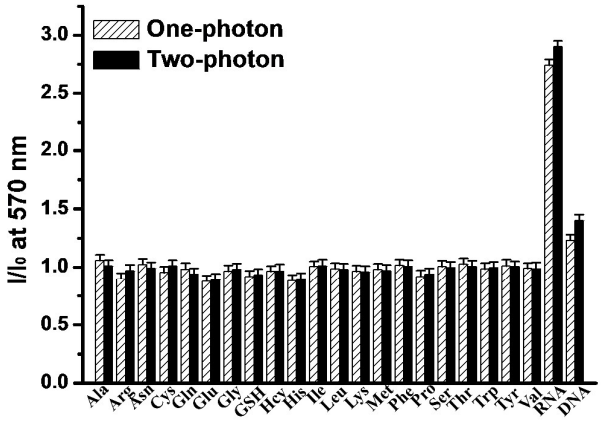

Fig. 6 One-photon and two-photon fluorescence responses of **OTP-ZnCl$_2$** (10 μM for one-photon fluorescence and 0.1 mM for two-photon fluorescence) toward various amino acids and NA (2 mM for one-photon fluorescence and 20 mM for two-photon fluorescence) in Tris-HCl buffer (pH 7.4).

High selectivity is very important for an excellent chemosensor. Hence, one- and two-photon fluorescence spectra studies of the selective response of **OTP-ZnCl$_2$** has been carried out on other amino acids. As shown in **Fig 6**, no detectable changes in emission spectra of **OTP-ZnCl$_2$** was observed upon the additions of amino acids, such as alanine (Ala), arginine (Arg), cysteine (Cys) et al, indicating a high selectivity of **OTP-ZnCl$_2$** in sensing RNA.

2.5 Two-photon fluorescent imaging

MTT assay

As high cell viability is essential for biological applications, cytotoxicity test was run *via* the 3-(4,5-dimethylthiazol-2-yl)-2,5-diphenyltetrazilium bromide (MTT) assay in different cells (HepG2, A549, MCF-7 and 3T3) cells. **Fig S8** demonstrated that after over 6 hours' incubation with **FTP**, **OTP, FTP-ZnX$_2$** or **OTP-ZnX$_2$** (X=Cl, Br, I), high cell viability was obtained at the concentrations between 5 μM and 60 μM with all the compounds. This result elucidated that **FTP**, **OTP, FTP-ZnX$_2$** and **OTP-ZnX$_2$** (X=Cl, Br, I) exhibit low toxicity against living cells.

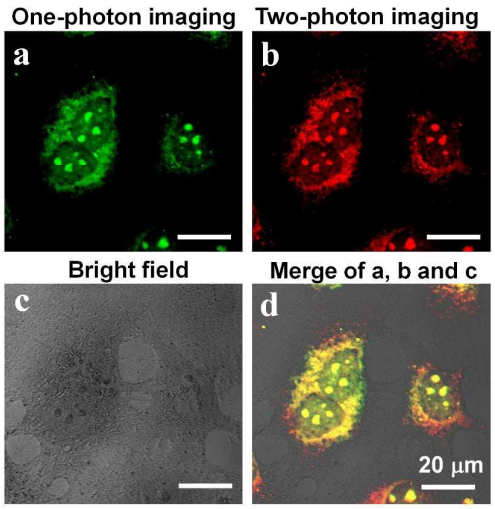

Fig. 7 The confocal fluorescence imaging of living HepG2 cells incubated with 30 μM **OTP-ZnCl$_2$** for 30 min. (a) The one-photon image of HepG2 cells (excited at 405 nm and emission collected in 510-570 nm). (b) The two-photon image of HepG2 cells (excited at 820 nm and emission collected in 520-580 nm). (c) The bright field of HepG2 cells. (d) Merged image of a, b and c.

The cellular uptake properties

Cellular uptake is critical to the success of a compound as intracellular probe. HepG2 cells as a model were incubated with 30 μM **FTP**, **OTP, FTP-ZnX$_2$** and **OTP-ZnX$_2$** (X=Cl, Br, I) for 30 min. Cells were then imaged using confocal microscopy after washing with PBS (×3). **Fig S9** and **Fig 7** showed that **FTP**, **OTP, FTP-ZnX$_2$** and **OTP-ZnX$_2$** (X=Cl, Br, I) could penetrate into the cell cytosol within short incubation period and displayed intensive luminescence in both one-photon and two-photon channels. It was noteworthy that **OTP-ZnCl$_2$** could enter the nuclear region and exhibited strong interaction with nucleoli. A similar intracellular distribution was observed in more cancerous cells (A549 and MCF-7 cells) and normal cells (3T3 cells) as representatives. As shown in **Fig S10**, the staining position, shape and nucleoli labelled by **OTP-ZnCl$_2$** correspond to the dense and dark-phase nucleolar region in bright field.

To further determine the possible cellular uptake mechanism of **OTP-ZnCl$_2$**, HepG2 cells were incubated with 30 μM **OTP-ZnCl$_2$** for 20 min at 4 ^{o}C, then washed and imaged immediately. The low temperature micrographs (**Fig S11**) showed that no luminescence was observed when the cells were incubated with **OTP-ZnCl$_2$** at this temperature, indicating that **OTP-ZnCl$_2$** enters cells *via* an energy-dependent pathway (e.g. endocytosis, active transport) and confirming that **OTP-ZnCl$_2$** was not a membrane-permeable molecule.

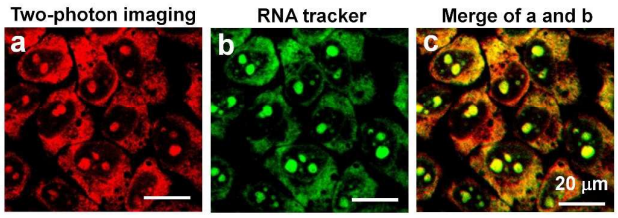

Fig. 8 Determination of intracellular localization of **OTP-ZnCl$_2$** by confocal microscopy. HepG2 cells were incubated with **OTP-ZnCl$_2$** (30 μM) for 30 min and then co-incubated with Syto9 (3 μM) for 15 min at 37 ^{o}C. (a) Two-photon image of **OTP-ZnCl$_2$**. (b) Confocal image of Styo9. (c) Merge image of a and b.

The subcellular localization of OTP-ZnCl$_2$

To understand the subcellular location of **OTP-ZnCl$_2$**, co-localisation studies of **OTP-ZnCl$_2$** with syto9 were conducted in HepG2 cells (**Fig 8**). Colocalization efficiency was quantified by using Pearson sample correlation factors (R_r). The intensity of the correlation plots revealed a high R_r value of 0.94, highly suggesting that **OTP-ZnCl$_2$** might have similar RNA binding efficiency as Syto9.

It is well known that the nucleolus contains abundant RNAs and RNA structural proteins, especially rRNA and ribosomal proteins. To further confirm whether **OTP-ZnCl$_2$** is RNA or DNA selective, a digestion test was performed with deoxyribonuclease (DNase I) and ribonuclease (RNase A). RNase is the enzyme that only hydrolyzes RNA and does not influence DNA, and vice versa. As shown in **Fig 9**, the two-photon fluorescence of **OTP-ZnCl$_2$** in cytoplasm and nucleoli was significantly diminished and tended to redistribute to the nucleoli comparing to the untreated samples. By contrast, after DNase digestion, the two-photon fluorescence of **OTP-ZnCl$_2$** in the nucleoli (mainly RNA) and cytoplasm (mainly ribosomal RNA) still remained. The confocal images revealed that **OTP-ZnCl$_2$** could selectively stain nucleoli and cytosolic RNA, which is further confirmed by quantitative flow cytometry analysis (**Fig S12**). As compared to the control cells, the **OTP-ZnCl$_2$**-treated cells exhibit higher fluorescence intensity. The RNase-treated cells show a decreased fluorescent intensity

while the DNase-treated cells present no obvious changed fluorescence intensity compared to **OTP-ZnCl$_2$**, suggesting that **OTP-ZnCl$_2$** preferring RNA to DNA.

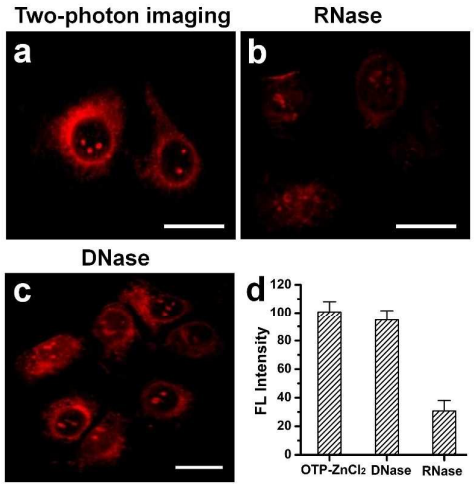

Fig. 9 The RNase and DNase digest experiments of **OTP-ZnCl$_2$** were operated by two-photon microscopy. HepG2 cells stained with **OTP-ZnCl$_2$** (30 μM) for 30 min before (a) or after treatment with RNase (25 μg/mL) (b) and DNase (30 μg/mL) (c) for 2h at 37 ^{o}C. (d) The relative two-photon fluorescence intensity of **OTP-ZnCl$_2$**, **OTP-ZnCl$_2$**+DNase and **OTP-ZnCl$_2$**+RNase. Scale bars = 20 μm.

NA are important biological macromolecules that function in encoding, transmitting, and expressing genetic information. The simultaneous visualization of DNA and RNA in nucleus is important using different dyes during the cell imaging. We investigated the counterstaining behavior using **OTP-ZnCl$_2$** with DNA dye Hoechst 33342. **Fig S13** showed the counterstain result of **OTP-ZnCl$_2$** and Hoechst 33342. The 2PM imaging from the nuclear zone with blue fluorescence means that **OTP-ZnCl$_2$** has good counterstain compatibility with Hoechst.

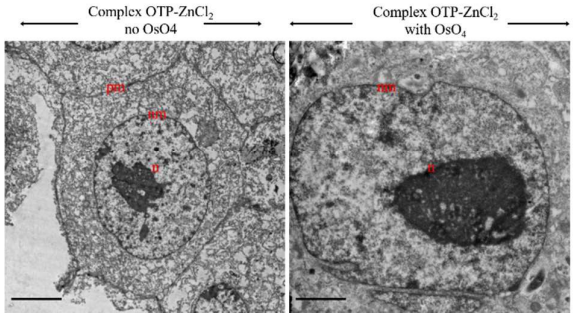

Fig. 10 Cellular localization of complex **OTP-ZnCl$_2$** characterized by transmission electron microscopy. TEM microscopy of HepG2 cells incubated with complex **OTP-ZnCl$_2$** and stained without osmium tetroxide (left). TEM microscopy of HepG2 cells incubated with complex **OTP-ZnCl$_2$** stained with osmium tetroxide (right). Abbreviations: nm=nuclear membrane, n= nucleolus, pm=plasma membrane. The scale bars=5μm.

In an attempt to more accurately determine the target of **OTP-ZnCl$_2$** with the organelles, HepG2 cells were incubated with **OTP-ZnCl$_2$** and then examined by transmission electron microscopy (TEM). As shown in **Fig 10**, although **OTP-ZnCl$_2$** was located throughout the cell cytosol, it was found in much higher concentration within the nucleoli of HepG2 cells. Despite of the lack of osmium tetraoxide, the TEM micrographs showed less membrane contrast, the nucleoli of fixed HepG2 cells were clearly stained by complex **OTP-ZnCl$_2$** after the incubation (**Fig 10**). These findings are again in agreement with the two-photon microscopy imaging, all strongly suggested that complex **OTP-ZnCl$_2$** has a superior interaction with intracellular RNA that were located within nucleoli in live cells.

2.6 Possible mechanism studies

The mechanism of selective nucleolus staining

To further investigate which component plays an important role in **OTP-ZnCl$_2$**, we chose **FTP**, **OTP**, **FTP-ZnX$_2$** (X=Cl, Br, I) and **OTP-ZnX$_2$** (X=Br, I) for a comparison. Compared with **FTP** (**Fig 4**), **FTP-ZnX$_2$** (X=Cl, Br, I) showed a stronger interaction with NAs. Moreover, **OTP** has a better interaction with RNA than DNA comparing to **FTP**. Though **OTP** and **OTP-ZnX$_2$** (X=Br, I) displayed a good interaction with NA in solution, only **OTP-ZnCl$_2$** was capable of entering the nuclear region.

The possible reasons for this mechanism were given as follows: (1) compared with the other complexes, **OTP-ZnCl$_2$** can cross the nuclear membrane due to the combined action between the oxime group and the chloride atoms. Chlorine has a smaller atomic radius than bromine and iodine atoms. Moreover, oxime group has a large amount of hydrogen bonds exist between RNA and hydrogen atoms. (2) some specific intracellular distribution and organization of RNA and DNA molecules can cause the difference in the affinity of **OTP-ZnCl$_2$** to DNA and RNA within cells.[23] (3) the structure of NA in solution may not exactly reflect their real state in living cells. According to the results above,

OTP-ZnCl$_2$ have higher selectivity for RNA than DNA in living cells.

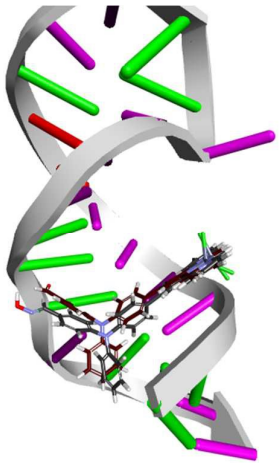

Fig. 11 LigandFit docking models obtained after molecular modeling for the interaction of **OTP-ZnCl$_2$** and **FTP-ZnCl$_2$** with RNA fragment (Aubergine represents **FTP-ZnCl$_2$**, gray represents **OTP-ZnCl$_2$**).

Molecular docking with RNA

Molecular docking techniques are very important tools in understanding the nature of RNA interaction in the molecule design, and in the mechanistic study. The molecular interaction between **OTP-ZnCl$_2$** and **FTP-ZnCl$_2$** with RNA are obtained through the method LigandFit docking. LigandFit docking is based on an initial shape match to the binding site, through a variety of scoring function (PMF, PLP and LigScore) to obtain the comprehensive Docking score, further get the highest score as well as the best Docking model. On the basis of the data obtained by the above, we conducted molecular modelling calculations using Discovery Studio 4.1 [41] with duplex RNA fragment (RNA ID: 2IXY, It's base sequences GGCCUCCAAGCUGUGCCUUGGGUGGCC). The docking results (**Fig 11**) indicate that **OTP-ZnCl$_2$** and **FTP-ZnCl$_2$** can bind to duplex RNA via insert model, which is in agreement with the results of fluorescence spectra change of **OTP-ZnCl$_2$** and **FTP-ZnCl$_2$** in the presence of RNA. In addition, as shown in **Fig S14** and **S15**, the molecule simulation indication hydrogen bonds existing between **OTP-ZnCl$_2$** and RNA between the oxime group and the base pair of RNA, while there is no hydrogen bond between **FTP-ZnCl$_2$** and RNA due to its lack of oxime group, resulting in **OTP-ZnCl$_2$** being inserted inside RNA in a stable configuration. This is in good agreement with the experiment outcomes. Thus, our molecular modelling studies throw light on the binding modes by which these complexes interact with RNA and complement the experiment observations.

Conclusion

In summary, a series of novel terpyridine Zn (II) complexes possessing two-photon absorption have been synthesized and characterized. The results indicate that different halide ions have different effect on their photophysical properties. Their photophysical properties were further confirmed by theoretical calculations. Complex **OTP-ZnCl$_2$** can traffic through both the plasma membrane and nuclear membrane and strongly interact with RNA in cytoplasm and nucleoli. Furthermore, the experimental results from two-photon fluorescence microscopy showed that **OTP-ZnCl$_2$** preferred RNA to DNA in cells, and localized within nucleoli and cytoplasm, which can be a potential dye for nucleic acid detection and intracellular fluorescence imaging. We demonstrated how this complex successfully targeted the subcellular organelles in living cells. Moreover, **OTP-ZnCl$_2$** was also found to have good counterstain compatibility with Hoechst and to be suitable for DNA-RNA colocalization experiments. With good cell permeability, low cytotoxicity and large two-photon action absorption cross section, **OTP-ZnCl$_2$** can be candidates as a selective RNA fluorescence probe in living cells.

Acknowledgment

This work was supported by grants from the National Natural Science Foundation of China (51372003, 21271004, 51432001, 21271003, 51472002 and 21501001), Ministry of Education Funded Projects Focus on returned overseas scholar, the Higher Education Revitalization Plan Talent Project (2013).

References

1 B. Shirinfar, N. Ahmed, Y. S. Park, G. S. Cho, I. S. Youn, J. K. Han, H. G. Nam and K. S. Kim, *J. Am. Chem. Soc.,* 2013, **135**, 90-93.
2 J. Wahlgren, T. D. L. Karlson, M. Brisslert, F. V. Sani, E. Telemo, P. Sunnerhagen and H. Valadi, *Nucleic. Acids. Research.,* 2012, 1-12.
3 T. H. Ho, K. X. Dang, S. Lintula, K. Hotakainen, L. Feng, V. M. Olkkonen, E. W. Verschuren, T. Tenkanen, C. Haglund, K. L. Kolho, U. K. Stenman and J. Stenman, *Nucleic. Acids. Research.,* 2014, 1-11.
4 M. R. Gill, J. Garica-Lara, S. J. Foster, C. Smythe, G. Battaglia and J. A. Thomas, *Nat. Chem.* 2009, 662-667.
5 C. K. K. Choi, J. M. Li, K. C. Wei, Y. J. Xu, L. W. C. Ho, M. L. Zhu, K. K. W. To, C. H. J. Choi and L. M. Bian, *J. Am. Chem. Soc.,* 2015, **137**, 7337-7346.
6 M. Y. Zheng, D. Librizzi, A. Kılıç, Y. Liu, H. Renz, O. M. Merkel and T. Kissel, *Biomaterials.,* 2012, **33**, 6551-6558.
7 G. F. Song, Y. M. Sun, Y. Liu, X. K. Wang, M. L. Chen, F. Miao, W. J. Zhang, X. Q. Yu and J. L. Jin, *Biomaterials.,* 2014, **35**, 2103-2112.
8 R. P. Haugland, In: Spence MTZ, editor. A guide to fluorescent and labeling technologies: the handbook. 10th ed. 2005, pp, 710-711.
9 X. Peng, F. Song, E. Lu, Y. Wang, W. Zhou, J. Fan and Y. Gao, *J. Am. Chem. Soc.,* 2005, **127**, 4170-4171.
10 L. Yuan, W. Lin, Y. Xie, B. Chen and J. Song, *Chem. Eur. J.,* 2012, **18**, 2700-2706.
11 S. Zhang, J. L. Fan, Z. Y. Li, N. J. Hao, J. F. Cao, T. Wu, J. Y. Wang and X. J. Peng, *J. Mater. Chem. B.,* 2014, **2**, 2688-2693.
12 L. Yuan, W. Lin, Z. Cao, J. Wang and B. Chen, *Chem. Eur. J.,* 2012, **18**, 1247-1255.
13 L. Li, X. Q. Shen, Q. H. Xu and S. Q. Yao, *Angew. Chem. Int. Ed.,* 2013, **52**, 424-428.
14 L. Li, J. Y. Ge, H. Wu, Q. H. Xu and S. Q. Yao, *J. Am. Chem. Soc.*, 2012, **134**, 12157-12167.
15 L. Li, C. W. Zhang, G. Y. J. Chen, B. W. Zhu, C. Chai, Q. H. Xu, E. K. Tan, Q. Zhu, K. L. Lim and S. Q. Yao, *Nat. Commun.,* 2014, **5**, 3276-3286.
16 K. L. A. Chan and S. G. Kazarian, *Chem. Soc. Rev.,* 2016, **45**, 1850-1864.
17 J. L. Li, F. F. Cheng, H. P. Huang, L. L. Li and J. J. Zhu, *Chem. Soc. Rev.,* 2015, **44**, 7855-7880.
18 J. tang, Y. B. Cai, J. Jing and J. L. Zhang, *Chem. Sci.,* 2015, **6**, 2389-2397.
19 D. L. Ma, H. Z. He, K. H. Leung, D. S. H. Chan and C. H. Leung, *Angew. Chem. Int. Ed.,* 2013, **52**, 7666-7682.
20 H. Y. Huang, L. Yang, P. Y. Zhang, K. Q. Qiu, J. J. Huang, Y. Chen, J. J. Diao, J. K. Liu, L. N. Ji, J. G. Long and H. Chao, *Biomaterials.,* 2016, **83**, 321-331.
21 Y. Ma, H. Liang, Y. Zeng, H. R. Yang, C. L. Ho, W. J. Xu, Q. Zhao, W. Huang and W. Y. Wong, *Chem. Sci.,* 2016, **7**, 3338-3346.
22 S. G. Sun, J. T. Wang, D. Z. Mu, J. Y. Wang, Y. M. Bao, B. Qiao and X. J. Peng. *Chem. Commun.,* 2014, **50**, 9149-9152.
23 H. Y. Huang, B. Yu, P. Y. Zhang, J. J. Huang, Y. Chen, G. Gasser, L. N. Ji and H. Chao, *Angew. Chem. Int. Ed.,* 2015, **54**, 14049-14052.
24 J. P. Liu, Y. Chen, G. Y. Li, P. Y. Zhang, C. Z. Jin, L. L. Zeng, L. N. Ji and H. Chao, *Biomaterials.,* 2015, **56**, 140-153.
25 E. Baggaley, M. R. Gill. N. H. Green, D. Turton, I. V. Sazanovich, S. W. Botchway, C. Smythe, J. W. Haycock, J. A. Weinstein and J. A. Thomas. *Angew. Chem. Int. Ed.,* 2014, **53**, 3367-3371.
26 N. A O'Connor, N. Stevens, D. Samaroo, M. R. Solomon, A. A. Martí, J. Dyer, H. Wishwasrao, D. L. Akins, E. R. Kandel and N. J. Turro. *Chem. Commun.,* 2009, 2640-2642.
27 K. Mitra, S. Gautam, P. Kondaiah and A. R. Chakravarty, *Angew. Chem. Int. Ed.,* 2015, **54**, 13989-13993.
28 S. W. Botchway, M. Charnley, J. W. Haycock, A. W. Parker, D. L. Rochester, J. A. Weinstein and J. A. G. Williams. *PNAS.,* 2008, **105**, 16071-16076.
29 S. I. Pascu, P. A. Waghorn, T. D. Conry, H. M. Betts, J. R. Dilworth, G. C. Churchill, T. Pokrovska, M. Christlieb, F. I. Aigbirhio and J. E. Warren. *Dalton. Trans.,* 2007, 4988-4997.
30 D. Xie, J. Jing, Y. B. Cai. J. Tang, J. J. Chen and J. L. Zhang, *Chem. Sci.,* 2015, **5**, 2318-2327.
31 Q. Zhang, X. H. Tian, Z. J. Hu, C. Brommesson, J. Y. Wu, H. P. Zhou, S. L. Li, J. X. Yang, Z. Q. Sun, Y. P. Tian and K. Uvdal, *J. Mater. Chem. B.,* 2015, **3**, 7213-7221.
32 C. C. Kong, M. H. Peng, H. Shen, Y. M. Wang, Q. Zhang, H. Wang, J. Zhang, H. P. Zhou, J. X. Yang, J. Y. Wu and Y. P. Tian, *Dyes and Pigemnts.,* 2015, **120**, 328-334.
33 R. Sakamoto, S. Katagiri, H. Maeda, Y. Nishimori, S. J. Miyashita and H. Nishihara, *J. Am. Chem. Soc.,* 2015, **137**, 734-741.
34 B. B. Cui, Y. W. Zhong and J. N. Yao, *J. Am. Chem. Soc.,* 2015, **137**, 4058-4061.
35 S. Bhowmik, B. N. Ghosh, V. Marjomäki and K. Rissanen, *J. Am. Chem. Soc.,* 2014, **136**, 5543-5546.
36 J. Liu, Q. Zhang, H. J. Ding, J. Zhang, J. Y. Tan, C. K. Wang, J. Y. Wu, S. L. Li, H. P. Zhou, J. X. Yang and Y. P. Tian, *Sci. China. Chem.,* 2013, **56**, 1315-1324.
37 M. Kong, T. Wang, X. H. Tian, F. Wang, Y. Q. Liu, Q. Zhang, H. Wang, H. P. Zhou, J. Y. Wu and Y. P. Tian, *J. Mater. Chem. C.,* 2015, **3**, 5580-5588.
38 H. Wang, Q. Zhang, J. Zhang, L. Li, Q. Zhang, S. L. Li, S. Y. Zhang, J. Y. Wu and Y. P. Tian, *Dyes and pigments.,* 2014, **102**, 263-272.
39 X. S. Zhao, J. Liu, H. Wang, Y. Zou, S. L. Li, S. Y. Zhang, H. P. Zhou, J. Y. Wu and Y. P. Tian, *Dalton. Trans.,* 2105, **44**, 701-709.
40 D. D. Li, X. H. Tian, A. D. Wang, L. J. Guan, J. Zheng, F. Li, S. L. Li, H. P. Zhou, J. Y. Wu and Y. P. Tian, *Chem. Sci.,* 2016, **7**, 2257-2263.
41 G. Wu, D. H. Robertson, C. L. Brooks III and M. Vieth, *J. Comput. Chem.,* 2003, **24**, 1549-1562.

An oxime-functionalized terpyridine $ZnCl_2$ complex is a RNA two-photon fluorescence probe exhibiting RNA binding, fluorescence intensity enhancement and compatible with DAPI.